International Journal of Coal Geology 183 (2017) 110–119

Contents lists available at ScienceDirect

International Journal of Coal Geology

journal homepage: www.elsevier.com/locate/coal

Effect of ion milling on the perceived maturity of shale samples: Implications for organic petrography and SEM analysis

M. Mastalerz[a,*], J. Schieber[b]

[a] Indiana Geological and Water Survey, Indiana University, 611 N. Walnut Grove Ave., Bloomington, IN 47405, USA
[b] IU Shale Research Lab, Department of Earth and Atmospheric Sciences, Indiana University, 1001 E. 10th St., Bloomington, IN 47405, USA

ARTICLE INFO

Keywords:
Ion milling
SEM
Maturity
New Albany Shale

ABSTRACT

Sample polishing by argon ion beam is a widely used method for examining shale samples for inherent porosity characteristics; the high quality of these surfaces suggests that this technique may also be used for optical reflectance measurements to provide information about the thermal maturity of samples. Yet, the inevitable surface heating that this polishing method engenders has raised concerns that the measured reflectance properties are no longer those of the original sample. To explore the impact of ion milling on the maturity of shale samples as measured by vitrinite and solid bitumen reflectance, five different ion milling configurations were applied to a set of organic-rich New Albany Shale (Late Devonian-Early Mississippian) samples that range in maturity from immature to post-mature. Using two ion mill designs, edge milling vs planar milling, single and dual ion beams, variable acceleration voltages, and milling at room temperature vs samples cooled by liquid nitrogen, provided a wide range of beam heating scenarios. Reflectance of macerals was measured before and after ion milling to investigate whether and to what extent various ion-milling approaches change the reflectance values, and by extension the perceived thermal maturity of organic matter in these samples. Our results demonstrate that more aggressive milling methods, such as the use of multiple beams and higher acceleration voltages elevate reflectance values, and that this effect is most pronounced in immature samples and diminishes for samples of increasing original maturity. Specifically, for the two least mature samples, the most aggressive milling method (configuration D) increased reflectance of vitrinite from 0.48% to 0.58%, and from 0.58% to 0.74%. Increase of reflectance (perceived maturity) can be counteracted by reducing beam intensity (e.g., fewer beams, lower voltage) and cooling of samples with liquid nitrogen. The severity of heating artifacts depends partially on the ion mill design, and non-damaging settings must be determined experimentally for a given ion mill model. Because thermal alteration of organic matter typically involves the expulsion of volatiles, there is also a danger that ion beam heating of immature and oil window samples can skew the porosity characteristics of shale samples. Thus, determining non-damaging ion mill settings has the dual benefit of avoiding measuring false maturity levels and misleading porosity characteristics.

1. Introduction

Over the last few decades, scanning electron microscopy (SEM) of argon ion milled samples has been increasingly used to study textural details, diagenetic transformations, and pore characteristics in shales. Argon ion milling is a sample preparation technique developed by material scientists (Bollinger and Fink, 1980) to avoid mechanical damage to surfaces to be studied for nanometer-scale details. In applications to shales, it has enabled the imaging of pore spaces and mineral relationships at magnifications beneficial to shale studies (Jiang et al., 1990; Hover et al., 1996; Rask et al., 1997; Schieber, 1998, 2002). Argon ion milling is now the technique of choice for the study of shale porosity (Tomutsa et al., 2007; Loucks et al., 2009; Schieber, 2010, 2011), because it provides high-quality, undistorted, flat sections of shale samples that allow high-quality SEM imaging and characterization of nanopores (Desbois et al., 2009; Curtis et al., 2012, 2014; Klaver et al., 2015).

Ion-milled surfaces can be prepared with either stand-alone ion mills that are marketed by several equipment manufacturers in a range of configurations or also with dual-focus ion beam/SEM machines that are available from major manufacturers of electron microscopes. With the latter methodology, a 30 kV ion beam is applied to a very small sample area (tens of microns) for serial sectioning and imaging (Curtis et al., 2012; Bernard et al., 2013; Klaver et al., 2015).

* Corresponding author.
E-mail address: mmastale@indiana.edu (M. Mastalerz).

http://dx.doi.org/10.1016/j.coal.2017.10.010
Received 30 August 2017; Received in revised form 12 October 2017; Accepted 15 October 2017
Available online 16 October 2017
0166-5162/ © 2017 Elsevier B.V. All rights reserved.

Sample preparation by ion milling has recently come under scrutiny because of the possibility of changing rock surface characteristics as a result of sample heating by the ion beam (Ishitani et al., 2004; Mayer et al., 2007; Knipling et al., 2010). Sanei and Ardakani (2016), using a cryogenic broad ion beam (BIB) and focused ion beam (FIB) on mudrocks, documented significant increases in reflectance values of macerals, up to one order of magnitude difference using the high energy FIB. Arango and Katz (2017) also reported changes in maturity and generation of solid bitumen on SEM-analyzed ion-milled surfaces. In contrast, Grobe et al. (2017) claimed that a systematic increase in reflectance was not observed if the correct polishing method was used.

We have previously conducted tests to evaluate the potential impact of ion milling on organic matter (OM) porosity characteristics (Schieber et al., 2016) and found that, with appropriate kV settings and liquid nitrogen cooling, we were able to avoid ion milling artifacts (e.g., possibility of producing artificial pores) that otherwise would have negatively affected our assessment of OM porosity. Consequently, we were curious about the potentially adverse effects of a given ion milling method on maturity measurements made on vitrinite and bitumen in shales. Specifically, if ion milling of shales changes the reflectance characteristics of organic matter and leads to the generation of bitumen during ion milling, it may potentially affect visual porosity assessments (solid bitumen occluding pores) and also determinations of thermal maturity. Numerous highly cited papers that discuss porosity characteristics have used SEM imaging of ion-milled surfaces as key evidence for their interpretations (e.g., Curtis et al., 2011; Fishman et al., 2012; Milliken et al., 2013; Loucks and Reed, 2014; see also papers in Camp et al., 2013). A substantial number of prior studies of maturity and porosity could be affected by the way surfaces have been milled, and so it seems prudent to investigate this matter at some depth.

2. Methods

A set of five New Albany Shale (Late Devonian-Early Mississippian) samples, ranging from immature to post-mature were used in this study (Table 1). These are organic-rich samples that contain abundant liptinite in samples IN-7, IL-6, and IN-2 and abundant solid bitumen in samples IL-1 and IL-3 (Fig. 1). The organic macerals were first examined on mechanically polished surfaces by standard organic petrography for reflectance and maturity, and then sample splits were ion milled in multiple configurations. For each configuration, reflectance was again determined optically.

For organic petrographic analysis and maturity determination, sample preparation techniques followed standard organic petrography procedures (Taylor et al., 1998). For reflectance analysis (R_o random) of the original samples, 25 measurements were collected. For ion-milled samples (especially edge-milled), the number of reflectance measurements varied depending on the size of the available surface area. Reflectance of vitrinite and solid bitumen was measured on all samples, and reflectance of amorphous organic matter (bituminite) was measured when present. A Leica DM 2500P microscope linked to a TIDAS PMT IV photometric system was used for these analyses, utilizing both white reflected light and fluorescent light.

Ion milling was conducted in the Indiana University (IU) Shale Research Lab with two types of ion mills—GATAN 600 Duomills and a GATAN Ilion. The GATAN 600 is a rather venerable piece of equipment that is no longer manufactured. These mills were initially designed to process samples for transmission electron microscopy (TEM) observations, and have proven so durable that many are still in service in laboratories; they are still available from various vendors of used lab equipment. We have two in operating condition and use them routinely, but not as initially intended. Because TEM samples are very thin and fragile and easily damaged by the SEM beam, we redesigned the sample holders so that we can mill 12.5 mm diameter surfaces on thin slices (2 mm thick) of shale (Schieber, 2010, 2013; Schieber et al., 2016). Milled surfaces were mechanically polished using successively finer grit (as fine as 1 μm) and were then milled for 2 h at 4 kV and a beam incident angle of 7.5°. This approach produced smooth surfaces for later examination by petrographic microscope, the measurement of reflectance, and pore studies.

The GATAN 600 (Fig. 1A) is a broad beam mill, and in our configuration we use a single beam on a rotating sample of up to 12.5 mm diameter (Fig. 1B). As shown in Fig. 1D, the beam dissipates away from the source aperture, and a rather broad area of the sample (3–5 mm wide) interacts with the beam (Fig. 1E). A benefit of this characteristic is a comparatively "gentle" milling action and good heat dissipation across the sample surface. In addition, the sample is mounted (contact area 122 mm^2) in a metal holder that itself has a large contact area with the metal stage of the ion mill; this effectively counteracts heat buildup in the sample during milling. To further reduce heating artifacts, the sample stages can be thermally connected (via copper rod) to a liquid nitrogen reservoir; however, in this study there was no apparent need for additional cooling (see below).

The GATAN Ilion ion mills (Fig. 2A) were introduced in 2010 in an edge mill configuration where the sample is affixed with conductive cement (silver paint) to a rotating Ti sample holder (Fig. 2B, C). As the sample rotates, two beams (0° tilt) that cross near the sample edge are

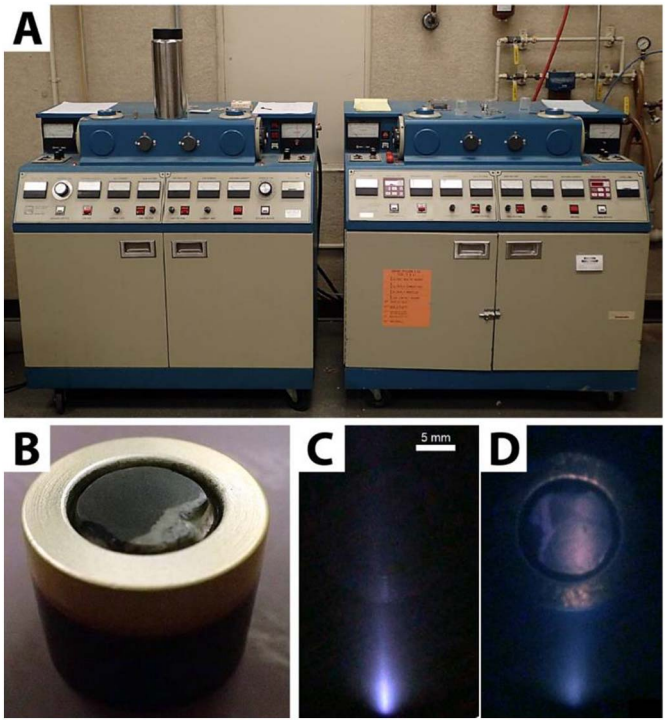

Fig. 1. (A) GATAN 600 Duomills in the Indiana University Shale Research Lab. Each mill can process two samples simultaneously. (B) Brass sample holder with sample in interior. Internal diameter of the holder is 12.5 mm. (C) View of ion beam without sample in chamber. Note how beam dissipates away from cathode aperture (at bottom). (D) View of ion beam interaction with sample. Note broad beam interaction (sample rotates under beam).

Table 1
Maturity (expressed by vitrinite reflectance, $R_{orandom}$), total organic carbon (TOC), total sulfur (TS) of the New Albany Shale samples. TOC and TS were analyzed using LECO SC832DR carbon/sulfur analyzer.

Sample	R_o (%)	TOC (weight %)	TS (weight %)
IN-7	0.48	7.8	3.3
IL-6	0.58	7.6	4.1
IN-2	0.72	2.9	6.5
IL-1	1.16	3.0	7.1
IL-3	1.40	0.61	3.3

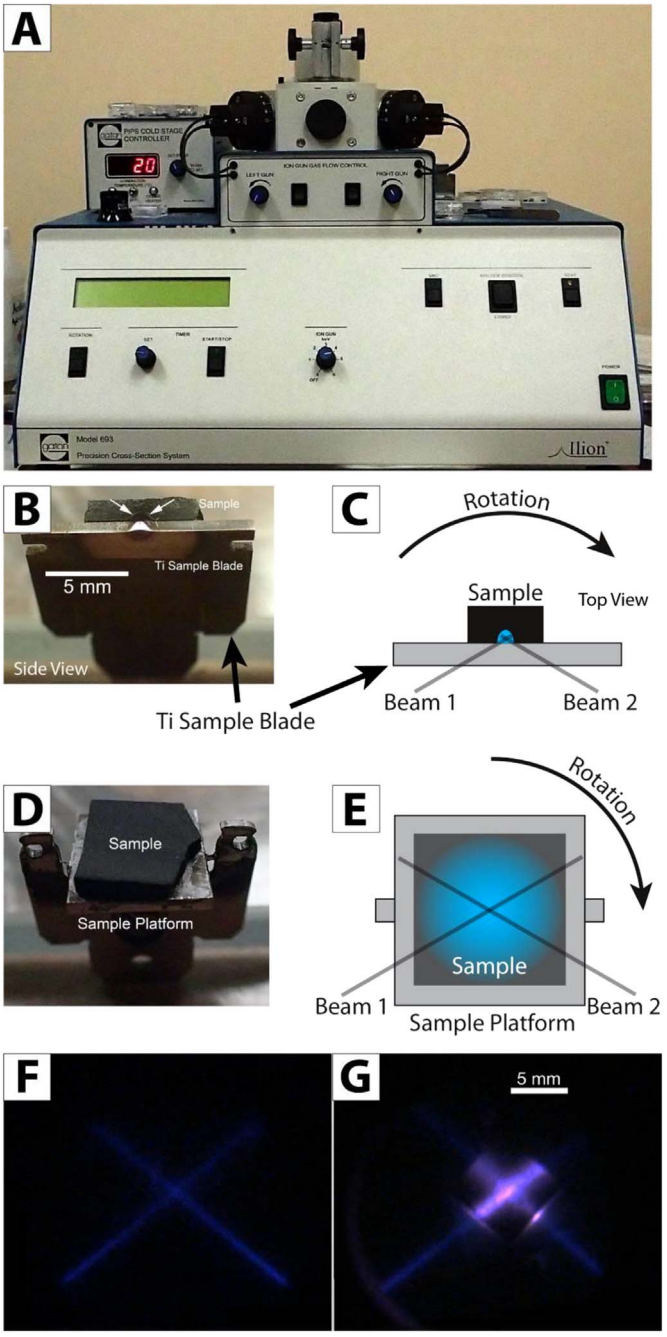

Fig. 2. (A) The 2010 model of the GATAN Ilion ion mill. (B) A sample holder (blade) for edge milling. Milled area is semicircular (arrows) and typically no larger than 1–2 mm^2. (C) Geometry of beams vs sample surface. (D) Sample holder for planar milling with sample. (E) Sketch of sample holder from D. (F) View of ion beams without sample in chamber. Note that beams are much narrower and disperse less compared to the GATAN 600 beam (Fig. 1). (G) View of beam interaction with sample. Note that interaction zone for each beam is distinctly narrower than that of the GATAN 600 mill (Fig. 1D).

alternately turned on and off as they face the sample blade (Fig. 2C). The beams operate over a 60° interval, and thus the sample receives beam energy for only a third of each rotation. Subsequently, a modified sample holder was introduced that allows planar milling, comparable to the approach taken in the GATAN 600 models (Fig. 2D, E). However, beams intersect in the middle of the sample and operate continuously as the sample rotates. The GATAN Ilion generates its beams with Penning guns that provide magnetic confinement of the beam. As a result, the beam is much narrower than that of the GATAN 600, and shows less dispersion away from the gun (Fig. 2F). Consequently, the beam interaction with the sample is narrower (and more intense) (Fig. 2G).

Because our objective was to determine ion mill configurations (Table 2) that would not alter the reflectance and maturity values previously measured on mechanically polished samples, we started the search by using a configuration (configuration A, Table 2) that we knew from past testing did not produce porosity artifacts in OM (Schieber et al., 2016). We then worked through other configurations that were feasible with our equipment base (Table 2). The milled surfaces were examined by SEM for visible artifacts, such as heat-damaged OM, formation of blisters and pseudo-pores, thermal shrinkage of OM, and thermal fracturing of minerals. Because direct measurements of heat are not possible for all configurations, in Table 2 "intensity" represents a qualitative estimate of the perceived amount of surface heating at a given configuration. We note that from measurements that we attempted in the past using infrared remote thermometers and temperature sensitive waxes, we can generally say that surface temperatures in the 120 to 140 °C range should be expected. Similarly, the precise rate of ion milling is not easily obtained because it depends on multiple factors such as thickness of material removed, composition of the rock being milled, and the beam energy and the incident angle. For edge milled samples, for example, a general rate of (lateral) advance of the milling front would be anywhere from 1 to 3 μm/min. For planar milled samples the vertical rate of sample removal is likely to be in the 0.1 to 1 μm/min range for quartz-rich and well cemented vs TOC and clay-rich samples, respectively.

3. Results

3.1. SEM surfaces

Although different milling regimes (Table 2) impart a range of thermal energy levels to the milled surfaces, the surfaces do not show an abundance of obvious thermal artifacts, such as thermal shrinkage, formation of blisters and pseudo-pores in OM, and thermal fracturing. To illustrate this, a collection of SEM images for the lowest-maturity sample (IN-7; Table 1) is shown in Fig. 3. The surfaces show a smooth polish and the OM is uniformly flat without signs of surface damage that might be due to heating by either the ion beam or the SEM beam. The other samples are of higher maturity (Table 1), and they show comparable surface quality across the range of milling conditions.

3.2. Reflectance values

Our data on a suite of samples having R_o values ranging from 0.48% to 1.41% ion milled at different conditions indicate that ion milling can

Table 2
Ion milling configurations.

Milling configuration		Milling conditions
A	GATAN 600, broadbeam, planar	12.5 mm sample rotates under single beam, room temperature. 7.5° inclination, 4 kV, 2 h, intensity level 1
B	GATAN Ilion, edge mill 1	Sample on Ti-blade, rotating, room temperature, 2 beams alternating, 0° inclination, 5 kV, 7 h, intensity level 1–2
C	GATAN Ilion, edge mill 2	Sample on Ti-blade, rotating, liquid nitrogen cooling, 2 beams alternating, 0° inclination, 5 kV, 7 h, intensity level 1
D	GATAN Ilion, planar 1	Sample chip on horizontal holder, rotating, room temperature, 2 beams simultaneous, 2° inclination, 5 kV, 2 h, intensity level 3
E	GATAN Ilion, planar 2	Sample chip on horizontal holder, rotating, liquid nitrogen cooling, 2 beams simultaneous, 2° inclination, 5 kV, 2 h, intensity level 2
F	GATAN Ilion, planar 3	Sample chip on horizontal holder, rotating, liquid nitrogen cooling, 2 beams simultaneous, 2° inclination, 4 kV, 2 h, intensity level 1–2

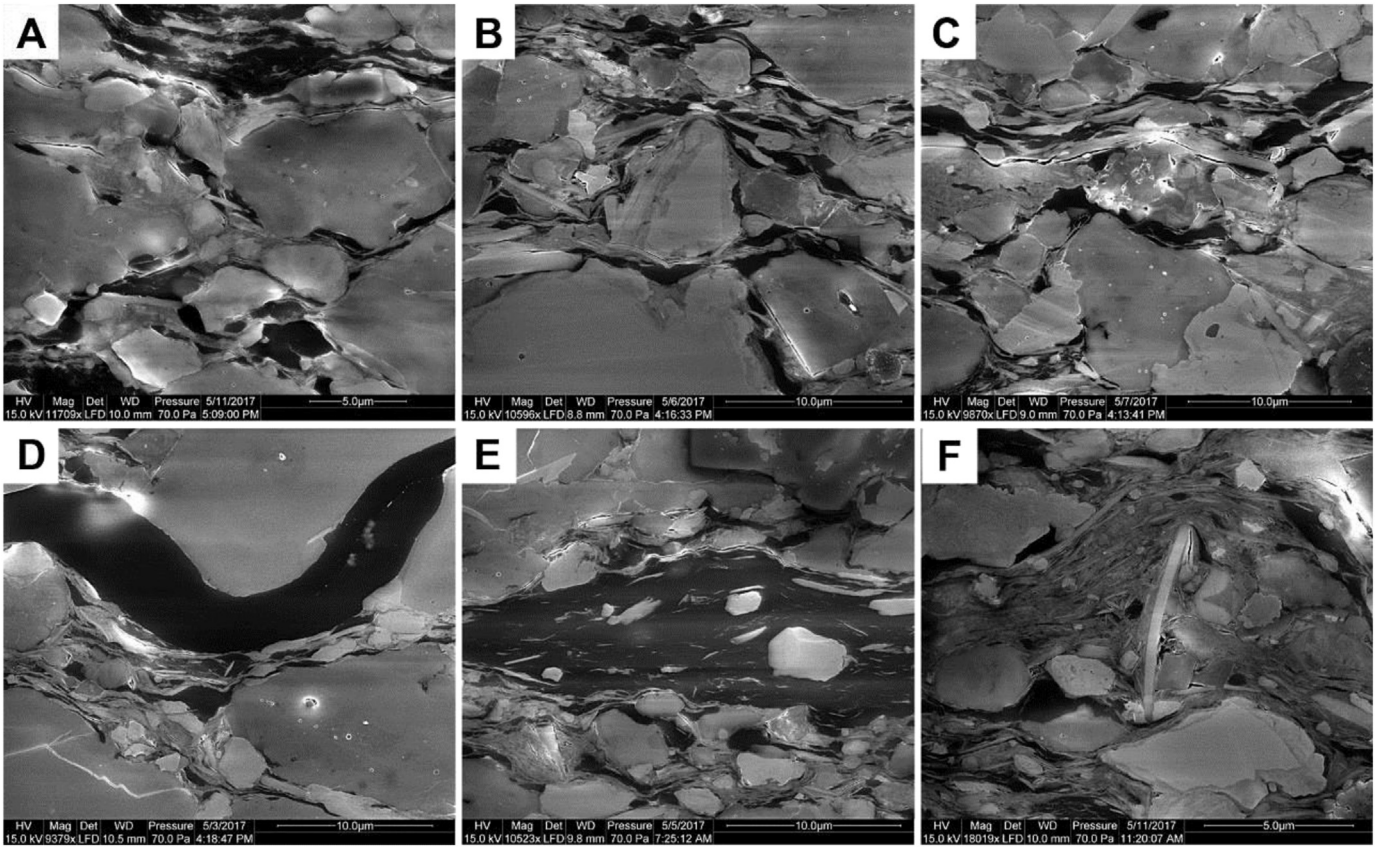

Fig. 3. Examples of ion milled surfaces from splits of sample IN-7. The A–F figure labels correspond to the milling configuration in Table 2. (A) This sample probably experienced the least intensive heating by the ion beam (GATAN 600, one beam, 4 kV, flat, RT), whereas (D) (Ilion, two beams, 5 kV, flat, RT) probably was heated the most. Because the samples were not coated and the SEM operated in low vacuum mode, there is some charging (bright spots) on disruptions on the surface, such as pores and microfractures. On photomicrographs, black and gray colors represent organic matter and minerals, respectively.

Table 3
Vitrinite reflectance (R_o, %) of the studied samples using different ion milling configurations. Values in parentheses are standard deviations.

Milling configuration	IN-7	IL-6	IN-2	IL-1	IL-3
Original R_o	0.48 (0.023)	0.58 (0.024)	0.72 (0.067)	1.16 (0.088)	1.41 (0.115)
Configuration A (G 600, Flat, RT)	0.49 (0.027)	0.60 (0.035)	0.71 (0.076)	1.14 (0.055)	1.38 (0.094)
% Increase from original value	*2.1*	*3.4*	*No increase*	*No increase*	*No increase*
Configuration B (Ilion, Edge, 5 kV, RT)	0.51 (0.031)	0.64 (0.043)	0.72 (0.029)	1.12 (0.021)	1.40 (0.093)
% Increase from original value	*6.3*	*10.3*	*No increase*	*No increase*	*No increase*
Configuration C (Ilion, Edge, 5 kV, LN2)	0.51 (0.016)	0.63 (0.051)	0.70 (0.031)	1.16 (0.0250	1.38 (0.088)
% Increase from original value	*6.3*	*8.6*	*No increase*	*No increase*	*No increase*
Configuration D (Ilion, Flat, 5 kV, RT)	0.56 (0.045)	0.74 (0.059)	0.76 (0.050)	1.20 (0.055)	1.41 (0.073)
% Increase from original value	*16.7*	*27.6*	*5.6*	*3.4*	*no increase*
Configuration E (Ilion, Flat, 5 kV, LN2)	0.52 (0.023)	0.73 (0.046)	0.71 (0.052)	1.22 (0.103)	1.41 (0.123)
% Increase from original value	*8.3*	*25.9*	*No increase*	*5.2*	*1.7*
Configuration F (Ilion, Flat, 4 kV, LN2)	0.49 (0.031)	0.68 (0.058)	0.71 (0.050)	1.18 (0.091)	1.40 (0.122)
% Increase from original value	*2.1*	*17.2*	*No increase*	*1.7*	*No increase*

RT = room temperature; LN2 = liquid nitrogen cooled.

change vitrinite reflectance on the sample surface and that the magnitude of change depends on the intensity of heating imparted by milling. Specifically, ion-milling configuration D (two beams operating simultaneously at 5 kV) notably changed the measured R_o of samples IN-7, IL-6, and IN-2 (Table 3). The observed change is largest for the early mature sample IL-6 (from 0.58% to 0.74% R_o, 27.6% increase from the original value). The R_o histograms for vitrinite of these three samples (Figs. 4, 5, 6) show a systematic shift in R_o values as a result of this comparatively aggressive milling approach. For the mid-mature sample IN-2, a smaller change from 0.72% to 0.76% (5.6% increase from the original value) is noted. In contrast, for the higher-maturity samples IL-1 and IL-3, the observed changes in R_o are smaller to absent (Table 3). Cooling with liquid nitrogen reduced the reflectance changes, similar in effect to lowering accelerating voltage from 5 to 4 kV (Table 3). Differences observed in edge-milled samples were not as drastic. In part, this may be an effect of the much smaller milled surface (Fig. 2B) available for observation and, consequently, the smaller number of possible reflectance measurements (on the edge-milled samples, the surfaces were only 1–2 mm^2 compared to the up-to-100-mm^2 surfaces on planar-milled samples). On planar-milled samples (Table 2; Figs. 1B, 2D) typically at least 25 reflectance measurements were recorded, whereas for edge-milled samples typically only 10 measurements were possible.

Solid bitumen mimics the heating effects observed for vitrinite,

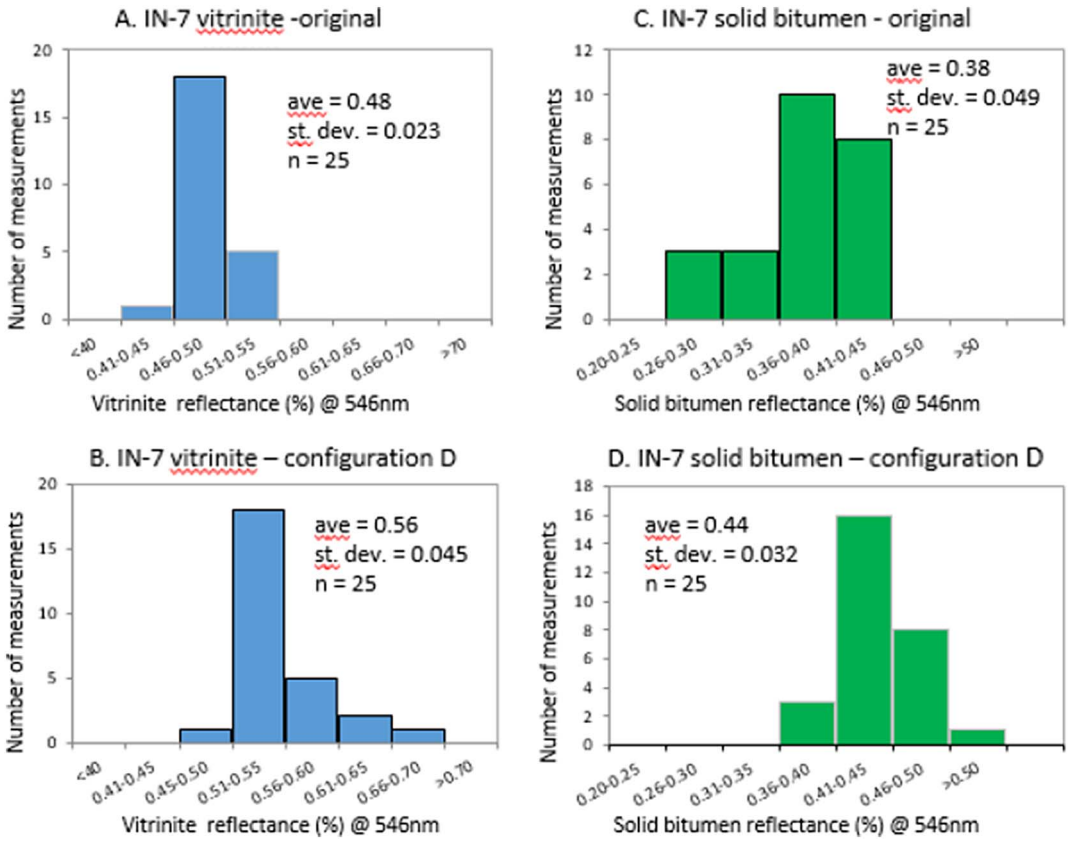

Fig. 4. Histogram of reflectance of vitrinite (A, B) and solid bitumen (C, D) in sample IN-7. Note the shift toward higher values (bottom row) in milling configuration D (planar, 2 continuous beams, Table 2) when compared to the original samples (top row). ave = average, st. dev. = standard deviation.

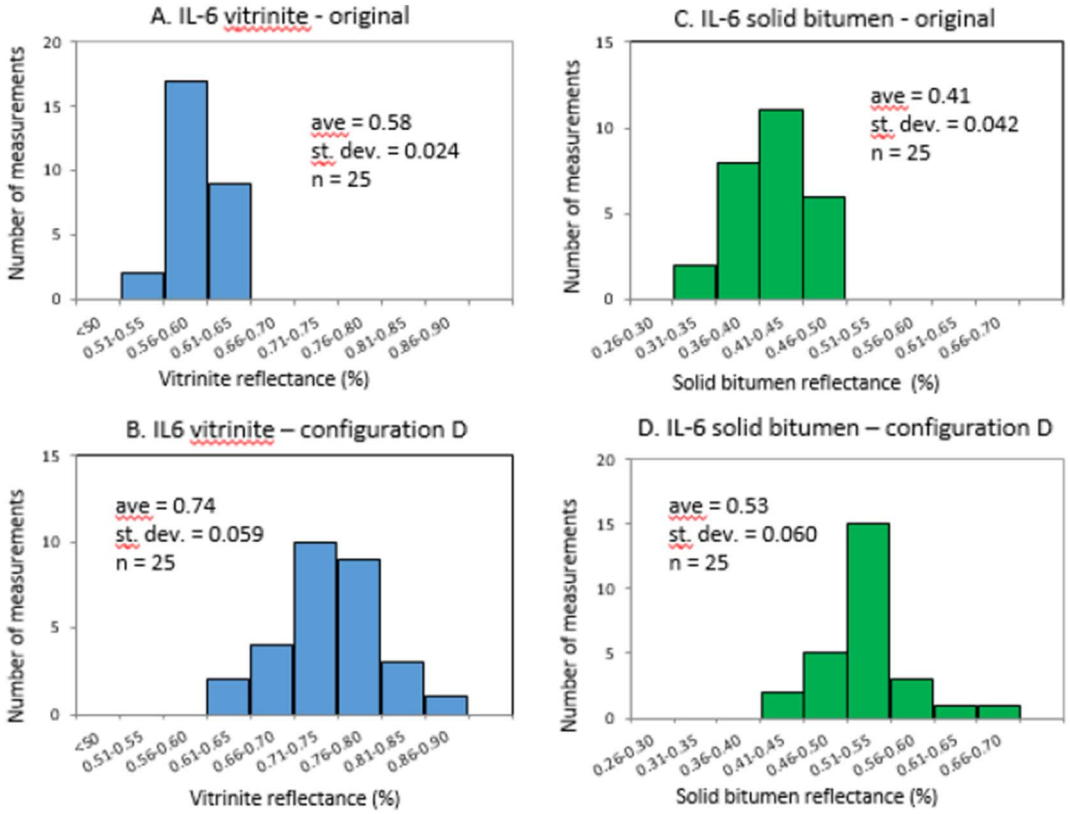

Fig. 5. Histogram of reflectance of vitrinite (A, B) and solid bitumen (C, D) in sample IL-6. Note a shift toward higher values (bottom row) in milling configuration D (planar, 2 continuous beams, Table 2) when compared to the original samples (top row). ave = average, st. dev. = standard deviation.

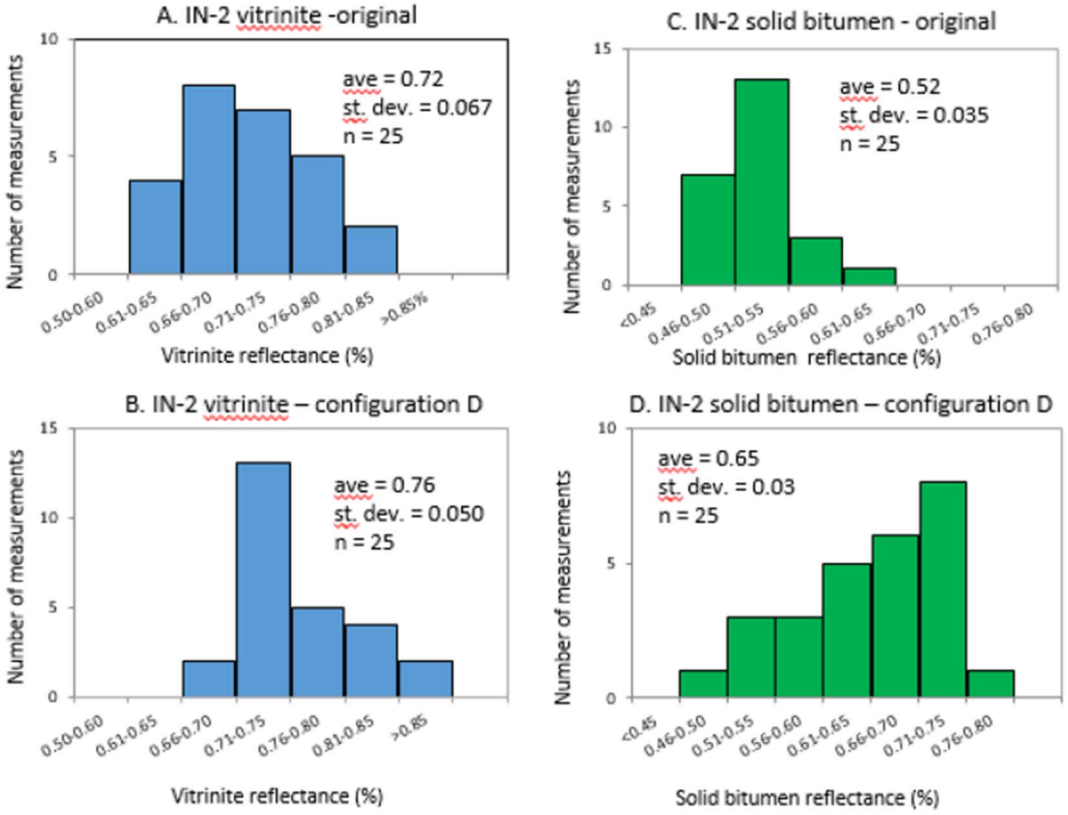

Fig. 6. Histogram of reflectance of vitrinite (A, B) and solid bitumen (C, D) in sample IN-2. Note a shift toward higher values (bottom row) in milling configuration D (planar, 2 continuous beams, Table 2) when compared to the original samples (top row). ave = average, st. dev. = standard deviation.

Table 4
Reflectance (R_o, %) of solid bitumen in the studied samples using different ion-milling configurations. Values in parentheses are standard deviations.

Milling configuration	IN-7	IL-6	IN-2	IL-1	IL-3
Original R_o	0.38 (0.049)	0.41 (0.042)	0.52 (0.035)	1.08 (0.123)	1.47 (0.081)
Configuration A (G 600, Flat, RT)	0.36 (0.037)	0.42 (0.059)	0.51 (0.050)	1.04 (0.093)	1.4 (0.106)
% Increase from original value	*No increase*	*2.4*	*No increase*	*No increase*	*No increase*
Configuration B (Ilion, Edge, 5 kV, RT)	0.38 (0.018)	0.45 (0.047)	0.52 (0.052)	1.10 (0.032)	1.40 (0.180)
% Increase from original value	*No increase*	*9.8*	*No increase*	*1.9*	*No increase*
Configuration C (Ilion, Edge, 5 kV, LN2)	0.41 (0.041)	0.44 (0.032)	0.52 (0.028)	1.17 (0.085)	1.37 (0.129)
% Increase from original value	*7.9*	*7.3*	*No increase*	*8.3*	*No increase*
Configuration D (Ilion, Flat, 5 kV, RT)	0.44 (0.032)	0.53 (0.060)	0.65 (0.073)	1.18 (0.117)	1.41 (0.090)
% Increase from original value	*15.8*	*29.3*	*23.1*	*9.3*	*No increase*
Configuration E (Ilion, Flat, 5 kV, LN2)	0.41 (0.031)	0.51 (0.059)	0.54 (0.055)	1.20 (0.109)	1.35 (0.072)
% Increase from original value	*7.9*	*24.4*	*3.8*	*11.1*	*No increase*
Configuration F (Ilion, Flat, 4 kV, LN2)	0.38 (0.031)	0.50 (0.087)	0.52 (0.050)	1.18 (0.109)	1.34 (0.179)
% Increase from original value	*No increase*	*22.0*	*No increase*	*9.3*	*No increase*

RT = room temperature; LN2 = liquid nitrogen cooled.

resulting in an elevated R_o for all except the most mature sample (IL-3) under the most aggressive ion-milling configuration D. The most affected samples (IN-7 [15.8% increase compared to the original sample], IL-6 [29.3% increase], IN-2 [23.1% increase]) show distinct shifts toward higher reflectance values (Table 4, Figs. 4, 5, 6). As observed for vitrinite, cooling with liquid nitrogen and lowering accelerating voltage reduced this effect (Table 4).

Reflectance of bituminite was measured in the two samples having the lowest maturity (IN-7 and IL-6). In the remaining sample, bituminite was either very dispersed, too small to measure (IN-2), or was not identified under the optical microscope (samples IL-1 and IL-3). In sample IN-7, reflectance of bituminite increased from 0.26% R_o in the original sample to 0.36% R_o (53% increase from the original value) after configuration D ion milling (Fig. 7A, B). In IL-6, R_o increased from 0.27% in the original sample to 0.45% R_o (66% increase) after configuration D ion milling (Fig. 7C, D).

3.3. Other observations

In reflected light, the surfaces of all samples looked very similar to those of the original samples after broad beam planar milling (configuration A), whereas after the most aggressive milling (configuration D), vitrinite was noticeably brighter in IL-6, and alginite in IN-2 changed from a brownish color in the original sample to a purple tint (Fig. 8A, B), probably a result of differing surface quality between ion-milled and mechanically polished surfaces. The surfaces of samples IL-1 and IL-3 looked like the original specimens after all types of ion milling (Fig. 8L, M).

In fluorescent light, no obvious changes in the intensity of fluorescence or fluorescent color of alginite were detected (Fig. 8D, E, G, H, J,

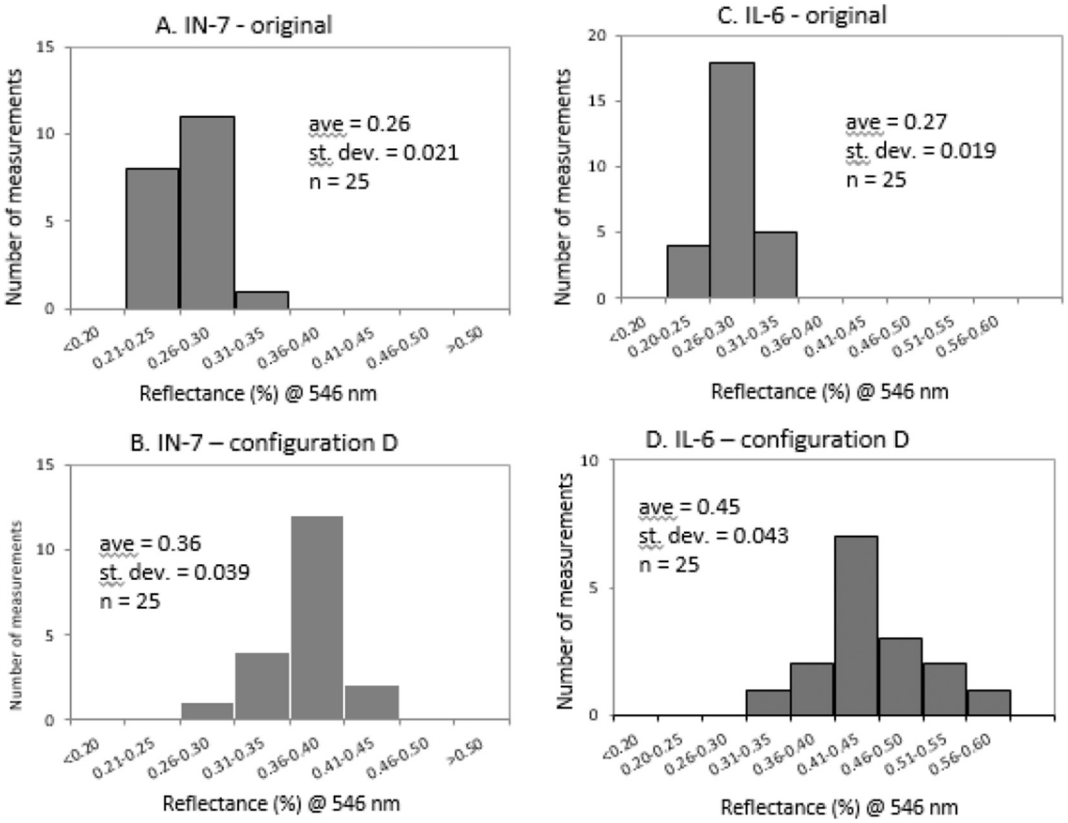

Fig. 7. Histogram of bituminite reflectance in sample IN-7 (A, B) and IL-6 (C, D). Note the shift toward higher values (bottom row) in milling configuration D (planar, 2 continuous beams, Table 2) when compared to the original samples (top row). ave = average, st. dev. = standard deviation.

K); small variations in color or intensity are explained by original differences or different sizes of alginite bodies. Although no point-counting was done to determine the proportions of different macerals, visually there was no notable increase in the amount of solid bitumen in the samples after ion milling, except sample IL-6, which showed an increased amount of solid bitumen at the expense of bituminite after the most aggressive (configuration D) treatment.

4. Discussion

Our study demonstrates that the way in which shale samples are ion milled influences the optically measured (maceral reflectance) maturity of organic matter. Thus, if ion-milled surfaces are to be used for maturity measurements, ion-milling conditions must be selected appropriately. Comparatively aggressive conditions, represented here by intensity level 3 (configuration D; Table 2) having two simultaneous beams and without liquid nitrogen cooling can cause significant shifts in perceived maturity levels as interpreted from R_o measurements, as seen in sample IN-7 (from immature to early mature) and sample IL-6 (from early mature to mid-mature). The observed increase in vitrinite reflectance is paralleled by an increase in the reflectance of solid bitumen and bituminite. The increase in reflectance of these macerals suggests molecular changes of OM, and in particular an increase in aromaticity, in response to heat buildup (e.g., Goodarzi and Murchison, 1978; Khavari-Khorasani and Michelson, 1993). In addition, the increase in the reflectance of bituminite from ~0.25% to 0.35% and 0.45% respectively in samples IN-7 and IL-6, indicates accelerated transformation of oil-prone kerogen into hydrocarbon products (Michelson and Khavari-Khorasani, 1990). The absence of noticeable changes in fluorescence color and fluorescence intensity of alginites in the immature and mid-mature samples (Fig. 8) is rather unexpected because an increase in reflectance typically is associated with changes in fluorescence intensity (e.g., Thompson-Rizer and Woods, 1987; Obermajer et al., 1999). This lack of correspondence indicates that the formation of multi-ring aromatic structural units from isolated aromatic rings that produced an increase in R_o (Carr and Williamson, 1990) is restricted to a very thin layer at the surface and does not affect the bulk molecular structure of the kerogen. This explanation has also been suggested in a study by Sanei and Ardakani (2016), who found no overall effect of ion milling on quantitative fluorescence parameters. In turn, Grobe et al. (2017) showed that a better surface quality achieved by broad ion milling resulted in higher reflectance values.

For higher maturity samples having vitrinite reflectance above 1%, minimal to no change in maturity was observed even after the most aggressive configuration D ion milling. This suggests that at this maturity level the oil-prone kerogen of the New Albany Shale is already well transformed (Mastalerz et al., 2013; Liu et al., 2017), has become more aromatic, and is therefore more resistant to heating. Collectively, these observations indicate that high-maturity samples are not as sensitive to ion-milling conditions as lower-maturity shales. However, even though the high-maturity shales in our study did not experience noticeable change in maturity, a study of pyrobitumen reflectance of the Montney Formation (Sanei and Ardakani, 2016) showed an increase from 2.16 to 2.38% when these shales underwent cryogenic broad ion beam milling at 6 kV. Judging from our own experience, the substantially higher beam energy (6 kV) may have been responsible for the increase. Thus, even in higher-maturity samples intense ion-milling conditions should be avoided to prevent the alteration of the sample surface.

Given that intense ion milling can clearly change the reflectance of OM, one has to wonder how ion milling might change the near-surface porosity of OM in shales. It has been well demonstrated that there is a significant change in porosity with maturation as a result of OM transformation and hydrocarbon generation (Jarvie et al., 2007; Loucks et al., 2009; Mastalerz et al., 2013), although this effect varies with regard to organic macerals (e.g., Schieber, 2013). Whereas the effect of

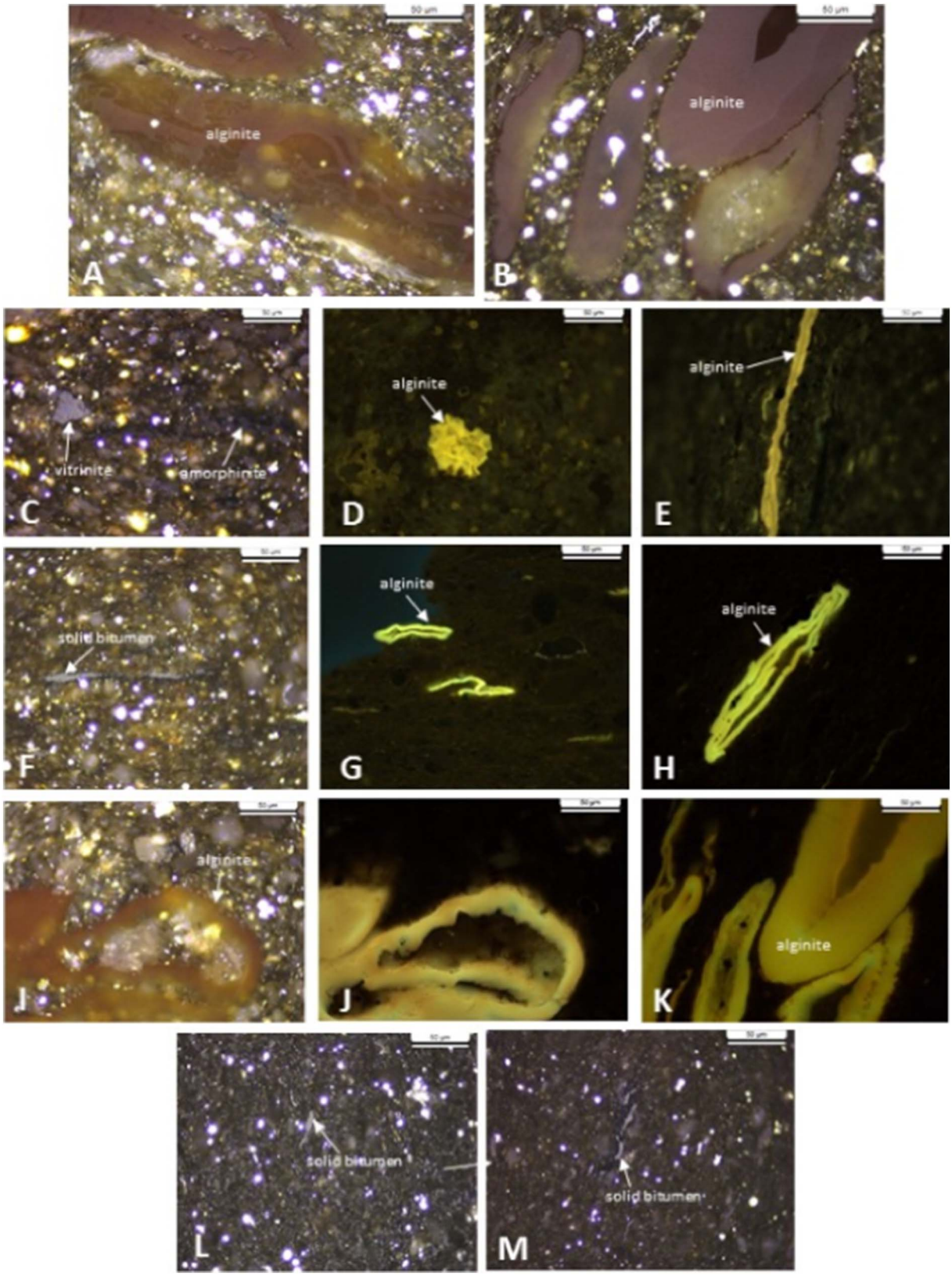

Fig. 8. Photomicrographs of studied samples. Reflected light images: A, B, C, F, I, L, M, fluorescent light images: D, E, G, H, J, K. (A) The original surface of sample IN-2. (B) The same surface after configuration D ion milling. Note the change in alginite color from brown to purple. (C) The original surface of sample IN-7. (D) Alginite in original sample IN-7. (E) Alginite in sample IN-7 after configuration D ion milling. (F) The original surface of sample IL-6. (G) Alginite in original sample IL-6. (H) Alginite in sample IL-6 after configuration D ion milling. (I) The original surface of sample IN-2. (J) Alginite in original sample IN-2, same field as I. (K) Alginite in sample IN-2 after configuration D ion milling. (L) The original surface of sample IL-1. (M) The original surface of sample IL-3. In all images the scale bar is 50 μm long. (For interpretation of the references to color in this figure legend, the reader is referred to the web version of this article.)

Table 5
Ion-milling conditions as reported in selected references.

Reference	Sample origin	Ion milling conditions reported
Grobe et al., 2017	Coal and graphite	5 kV for 10 min at 10.5° beam angle followed by 7 kV for 60 min at 3° beam angle.
Zhou et al., 2016	Silurian shales, Sichuan Basin	Electron beam and ion beam at 52° angle to each other, accelerating voltage 30 kV
Loucks and Reed, 2014	Various shales	Broad-beam, accelerating voltage 8 kV, gun current 2.8 mA
Schieber, 2013	Devonian Marcellus and New Albany shales	GATAN 600 Duomill, 4 kV, milled at 7.5° incident angle for 1–3 h
Milliken et al., 2013	Devonian Marcellus Shale	Argon-ion cross section polishing, accelerating voltage 8 kV, gun current 2.8 mA, milling time 10 h
Fishman et al., 2012	Upper Jurassic Kimmeridge Clay, North Sea	2.5 kV for 2 h followed by 1 kV for 1 h. Each ion milling step used a 40% focus, 5° tilt angle, and the samples were continuously rotated
Curtis et al., 2011	Marcellus shale	Initially 30 kV, 21 nA ion beam, later 920 pA current
Curtis et al., 2010	Various shales	FEI Helios NanoLab™ 600 DualBeam™ FIB-SEM, 30 kV
Loucks et al., 2009	Mississippian Barnett Shale	5–7 kV, gun current 300 μA

the heat generated because of the transfer of ion beam kinetic energy on the sample surface may be especially pronounced for OM (Bassim et al., 2012), the possibility of altering inorganic material by ion milling has also been raised (Phaneuf, 2005). Given that context, an additional question arises, namely, whether porosity data obtained by SEM observation of ion-milled surfaces are reliable. Although porosity effects are not the focus of this study, we do have some relevant information from prior studies (e.g., Schieber et al., 2016) that can give some basic guidance on this issue. Over the past decade, multiple studies concerned with shale porosity relied on SEM observations (Milliken and Curtis, 2016, and references therein), but those observations may have limited relevance if ion-milling conditions caused surface artifacts. As shown in Table 5, ion-milling conditions vary greatly between studies, different accelerating voltage and gun currents are used, and in some studies information about ion-milling conditions is limited or absent. It is, therefore, not easy to evaluate whether the pore observations were made on truly unaltered samples. This also hampers unbiased comparison between studies.

In past studies of shale porosity in the IU Shale Research Lab, the danger that pores might be generated in OM owing to ion-beam-heating was a serious concern (Schieber et al., 2016). To determine whether or not a given milling condition produced pore artifacts, the following step-wise procedure was adopted (Schieber et al., 2016). Step 1: Samples were given a mechanical high polish to 0.1 μm, cleaned gently, and then examined and imaged by SEM. Step 2: The samples were milled using a GATAN 600 DuoMill (Configuration A, Table 2) and again examined by SEM. The same areas as in Step 1 were again examined and imaged. Step 3: We compared images of mechanically polished vs ion-milled surfaces, and verified that the pores that were clearly visible once samples were ion milled were already visible on mechanically polished surfaces. Configuration A milling with the GATAN 600 DuoMill at room temperature did not produce significant changes of pore distribution, pore shape, or pore size, it merely made them stand out more clearly.

To further verify the previous results, the GATAN Ilion was used in configuration C (Table 2; edge mill, liquid nitrogen cooling) edge milling (Fig. 3), and the observed pore morphologies and densities were the same as observed with the GATAN 600 Duomill. In a final test, the GATAN Duomill was equipped with a liquid-nitrogen-cooled stage, and no differences to room temperature milling (configuration A, Table 2) were observed. Thus, the earlier tests suggest that both the GATAN Duomill and the GATAN Ilion can be operated at settings that are unlikely to produce porosity artifacts, and these settings coincide with operating conditions that prevent or minimize the formation of maturity artifacts. For other ion mill models than the ones we worked with, artifact-preventing operating conditions have to be determined experimentally; based on our experience, though, a general recommendation for best results is to use beam-accelerating voltages no higher than the 4 to 5 kV range, liquid nitrogen cooling, and shallow beam angles.

Because it appears that the relevant variable for producing maturity and porosity artifacts in OM is temperature and, thus, the current density of the ion beam, a general remedy might be to lower acceleration voltage even more when needed (2–3 kV is feasible), and to enhance sample cooling by using sample stages with high heat conductivity. For example, the current Ilion planar sample stage consists of stainless steel, a comparatively poor heat conductor because of its alloy structure. A stage made from aluminum or copper would be approximately 7 and 13 times, respectively, more conductive. In addition, the angle of beam incidence could be decreased. Spreading beam energy over a larger area in this way would require an increase in milling time, but this could be considered a necessary sacrifice if avoiding artifacts is the objective.

5. Conclusions

The conclusions that can be drawn from this study are as follows:

1) Ion milling can change the reflectance of the organic matter on the sample surface to various degrees, depending on the amount of beam energy imparted to the sample surface. The key variable in that regard is the current density of the ion beam, which can be controlled via acceleration voltage and incident angle. The temperature effects of the beam can also be counteracted by liquid nitrogen cooling and further ameliorated by high heat conductivity of the sample stage. Using fewer beams and/or discontinuously powered beams can also help to reduce heat loading of the sample surface.
2) Aggressive ion-milling configurations can affect reflectance measurements very significantly in immature and mid-mature samples. In samples having maturity above R_o = 1%, maturity changes are minor or absent, even with aggressive ion milling. In contrast, broad beam milling with a dissipative beam (GATAN 600) can produce unaltered smooth surfaces even at room temperature. If avoidance of artifacts, rather than milling speed, is an objective, appropriate milling configurations have to be determined experimentally for a given ion mill model.
3) Although this study did not focus on porosity artifacts in the examined sample set (Table 1), testing done in the context of prior porosity studies using the same ion mill configurations (Table 2) strongly suggest that ion-milling configurations that avoid maturity artifacts in immature and mid-mature samples are also appropriate settings for avoiding porosity artifacts.
4) A wide range of ion-milling conditions have been used in published studies of ion-milled shale surfaces, including settings that, in the context of our study, suggest a high risk of artifact generation (Table 5). It appears clear from our research that all such studies must provide the manner by which their samples were ion milled in detail, so that their results can be evaluated and compared in a meaningful way.

Acknowledgments

The presented data were acquired in the course of a study supported by the U.S. Department of Energy, Office of Science, Office of Basic Energy Sciences, Chemical Sciences, Geosciences, and Biosciences Division under Award Number DE-SC0006978. Additional support was provided by the sponsors of the IU Shale Research Consortium. We thank Paul C. Hackley and Ame Grobe for their thoughtful reviews of the paper.

References

Arango, I., Katz, B.J., 2017. Artificially-induced changes to organic matter properties as a consequence of the act of observation. In: AAPG Annual Convention and Exhibition, Houston, Texas, . http://www.searchanddiscovery.com/abstracts/html/2017/90291ace/abstracts/2597101.html.

Bassim, N.D., De Gregorio, B.T., Kilcoyne, A.L.D., Scott, K., Chou, T., Wirick, S., Cody, G., Stroud, R.M., 2012. Minimizing damage during FIB sample preparation of soft materials. J. Microsc. 245, 288–301.

Bernard, S., Brown, L., Wirth, R., Schreiber, A., Schulz, H.M., Horsfield, B., 2013. FIB-SEM and TEM investigations of an organic-rich shale maturation series from the Lower Toarcian Posidonia Shale, Germany: nanoscale pore system and fluid-rock interactions. In: Camp, W., Diaz, E., Wawak, B. (Eds.), Electron Microscopy of Shale Hydrocarbon Reservoirs. American Association of Petroleum Geologists Memoir 102. pp. 53–66.

Bollinger, D., Fink, R., 1980. A new production technique: ion milling. Solid-State Technol. 79–84.

Camp, W.K., Diaz, E., Wawak, B. (Eds.), 2013. Electron microscopy of shale hydrocarbon reservoirs. AAPG Mem. 102 (260 pp).

Carr, A.D., Williamson, J.E., 1990. The relationship between aromaticity, vitrinite reflectance and maceral composition of coals: implications for the use of vitrinite reflectance as a maturation parameter. Org. Geochem. 16, 313–323.

Curtis, M.E., Ambrose, R.J., Sondergeld, C.H., Rai, C.S., 2010. Structural characterization of gas shales on the micro- and nano-scales. In: Proceedings Canadian Unconventional Resources and International Petroleum Conference. Society of Petroleum Engineers, Calgary, Alberta (CUSG/SPE 137693).

Curtis, M.E., Ambrose, R.J., Sondergeld, C.H., Rai, C.S., 2011. Transmission and scanning electron microscopy investigation of pore connectivity of gas shales on the nanoscale. SPE Paper No 144391 In: Presented at North American Unconventional Gas Conference and Exhibition, The Woodlands, Texas, 14–16 June 2011.

Curtis, M.E., Cardott, B.J., Sondergeld, C.H., Rai, C.S., 2012. Development of organic porosity in the Woodford Shale with increasing thermal maturity. Int. J. Coal Geol. 103, 26–31.

Curtis, M.E., Georgen, E.T., Jernigen, J.D., Sondergeld, C.H., Rai, C.S., 2014. Mapping organic matter distribution on the centimeter scales with nanometer resolution. In: Proceedings Unconventional Resources Technology Conference, Denver, Colorado. SPE-AAPG-SEG., URTeC 1922757.

Desbois, G., Urai, J.L., Kukla, P.A., 2009. Morphology of the pore space in claystones–evidence from BIB-FIB ion beam sectioning and cryo-SEM observations. Earth 4, 15–22.

Fishman, N.S., Hackley, P.C., Lowers, H.A., Hill, R.J., Egenhoff, S.O., Eberl, D.D., Blum, A.E., 2012. The nature of porosity in organic-rich mudstones of the Upper Jurassic Kimmeridge Clay Formation, North Sea, offshore United Kingdom. Int. J. Coal Geol. 103, 32–50.

Goodarzi, F., Murchison, D.G., 1978. Influence of heating rate variation on the anisotropy of carbonized vitrinite. Fuel 57, 273–284.

Grobe, A., Schmatz, J., Littke, R., Klaver, J., Urai, J.L., 2017. Enhanced surface flatness of vitrinite particles by broad ion beam polishing and implications for reflectance measurements. Int. J. Coal Geol. 180, 113–121.

Hover, V.C., Peacor, D.R., Walter, L.M., 1996. STEM/AEM evidence for preservation of burial diagenetic fabrics in Devonian shales. J. Sediment. Res. 66, 519–530.

Ishitani, T., Umemura, K., Ohnishi, T., Yaguchi, T., Kamino, T., 2004. Improvements in performance of focused ion beam cross-sectioning: aspects of ion-sample interactions. J. Electron Microsc. 53, 443–449.

Jarvie, D.M., Hill, R.J., Ruble, T.E., Pollastro, E.M., 2007. Unconventional shale-gas systems: The Mississippian Barnett Shale of north-central Texas as one model for thermogenic shale-gas assessment. AAPG Bull. 91, 475–499.

Jiang, W.-T., Peacor, D.R., Essene, E.J., 1990. Transmission electron microscopic study of coexisting pyrophyllite and muscovite: direct evidence for the metastability of illite. Clay Clay Miner. 38, 225–240.

Khavari-Khorasani, G., Michelson, J.K., 1993. The thermal evolution of solid bitumens, bitumen reflectance, and kinetic modeling of reflectance: application in petroleum and ore prospecting. Energy Sources 15, 181–204.

Klaver, J., Desbois, G., Urai, J.L., Littke, R., 2015. BIB-SEM characterization of pore-space morphology and distribution in postmature to overmature samples from the Haynesville and Bossier Shales. Mar. Pet. Geol. 59, 451–466.

Knipling, K.E., Rowenhorst, D.J., Fonds, R.W., Spanos, G., 2010. Effects of focused ion beam milling on austenite stability in ferrous alloys. Mater. Charact. 61, 1–6.

Liu, B., Schieber, J., Mastalerz, M., 2017. Combined SEM and reflected light petrography of organic matter in the New Albany Shale: a perspective on organic porosity development with thermal maturation. Int. J. Coal Geol (in review).

Loucks, R.G., Reed, R.M., 2014. Scanning-electron-microscope petrographic evidence distinguishing organic-matter pores associated with depositional organic matter versus migrated organic matter. GCAGS. Journal 3, 51–60.

Loucks, R.G., Reed, R.M., Ruppel, S.C., Jarvie, D.M., 2009. Morphology, genesis, and distribution of nanometer scale pores in siliceous mudstones of the Mississippian Barnett Shale. J. Sediment. Res. 79, 848–861.

Mastalerz, M., Schimmelmann, A., Drobniak, A., Chen, Y., 2013. Porosity of Devonian/Mississippian New Albany Shale across a maturation gradient – insights from organic petrology, gas adsorption, and mercury intrusion. AAPG Bull. 97 (10), 1621–1643.

Mayer, J., Giannuzzi, L.A., Kamino, T., Michael, J., 2007. TEM sample preparation and FIB-induced damage. MRS Bull. 32, 400–407.

Michelson, J.K., Khavari-Khorasani, G., 1990. Monitoring chemical alterations of individual oil-prone macerals by means of microscopic fluorescence spectrometry combined with multivariate data analysis. Org. Geochem. 15, 179–192.

Milliken, K.L., Curtis, M.E., 2016. Imaging pores in sedimentary rocks: foundation of porosity prediction. Mar. Pet. Geol. 73, 590–608.

Milliken, K.L., Rudnicki, M., Awwiller, D.N., Zhang, T., 2013. Organic matter-hosted pore system, Marcellus Formation (Devonian), Pennsylvania. AAPG Bull. 97 (2), 177–200.

Obermajer, M., Stasiuk, L.L., Fowler, M.G., Osadetz, K.G., 1999. Application of acritarch fluorescence in thermal maturity studies. Int. J. Coal Geol. 39, 185–204.

Phaneuf, M.W., 2005. FIB for material science applications: a review. In: Giannuzi, L.A., Stevie, F.A. (Eds.), Introduction to Focus Ion Beams: Instrumentation, Theory, Techniques, and Practice. Springer, New York, pp. 143–172.

Rask, J.H., Bryndzia, L.T., Braunsdorf, N.R., Murray, T.E., 1997. Smectite illitization in Pliocene-age Gulf of Mexico mudrocks. Clay Clay Miner. 45, 99–109.

Sanei, H., Ardakani, O.H., 2016. Alteration of organic matter by ion milling. Int. J. Coal Geol. 163, 123–131.

Schieber, J., 1998. Deposition of mudstones and shales: overview, problems, and challenges. In: Schieber, J., Zimmerle, W., Sethi, P. (Eds.), Shales and Mudstones (vol. 1): Basin Studies, Sedimentology and Paleontology. Schweizerbart'sche Verlagsbuchhandlung, Stuttgart, pp. 131–146.

Schieber, J., 2002. Sedimentary pyrite: a window into the microbial past. Geology 30, 531–534.

Schieber, J., 2010. Common themes in the formation and preservation of intrinsic porosity in shales and mudstones–Illustrated with examples across the Phanerozoic. Paper number 132370-MS In: Society of Petroleum Engineers (SPE) Unconventional Gas Conference, 23–25 February 2010, Pittsburgh, Pennsylvania, USA.

Schieber, J., 2011. Shale microfabrics and pore development–an overview with emphasis on the importance of depositional processes. In: Leckie, D.A., Barclay, J.E. (Eds.), Gas Shale of the Horn River Basin. Canadian Society of Petroleum Geologists, Calgary, pp. 115–119.

Schieber, J., 2013. SEM observations on ion-milled samples of Devonian Black Shales from Indiana and New York: The petrographic context of multiple pore types. AAPG Mem. 102, 153–172.

Schieber, J., Lazar, R., Bohacs, K., Klimentidis, B., Ottmann, J., Dumitrescu, M., 2016. An SEM study of porosity in the Eagle Ford Shale of Texas – pore types and porosity distribution in a depositional and sequence stratigraphic context. AAPG Mem. 110, 153–172.

Taylor, G.H., Teichmüller, Davis A., Diessel, C.F.K., Littke, R., Robert, P., 1998. Organic Petrology. Gebrüder Borntraeger, Berlin, Stuttgart, pp. 704.

Thompson-Rizer, C.L., Woods, R.A., 1987. Microspectrofluorescence measurements of coals and petroleum source rocks. Int. J. Coal Geol. 7, 85–104.

Tomutsa, L., Silin, D., Radmilovic, V., 2007. Analysis of chalk petrophysical properties by means of submicron-scale pore imaging and modeling. SPE Reserv. Eval. Eng. 10, 285–293.

Zhou, S., Yan, G., Xue, H., Gao, W., Li, X., 2016. 2D and 3D nanopore characterization of gas shale in Longmaxi Formation based on FIB-SEM. Mar. Pet. Geol. 73, 174–180.